ARTICLE

# Geometry Dependence of Surface Plasmon Polariton Lifetimes in Nanohole Arrays

**Dang Y. Lei,[†,§] Jia Li,[‡,§] Antonio I. Fernández-Domínguez,[†,§] Hock C. Ong,[‡,*] and Stefan A. Maier[†,*]**

[†]Department of Physics, Imperial College London, London SW7 2AZ, United Kingdom, and [‡]Department of Physics, The Chinese University of Hong Kong, Shatin, Hong Kong. [§]These authors contributed equally to this work.

**ABSTRACT** We study surface plasmon polariton lifetimes in two-dimensional arrays of blind holes on gold surfaces. The lifetimes are determined from the line widths of the resonant dips appearing in the specular reflection spectra. We find a strong dependence of lifetimes on the resonant wavelength and the hole geometry. Through both experiments and numerical simulations, we analyze the validity of the Rayleigh approximation and also explore the range of wavelengths and geometric parameters where it fails. Finally, we show that, within the range of geometries and wavelengths considered in our experiments, the behavior of surface plasmon polariton lifetimes can be understood as resulting from the interplay between the intrinsic metal absorption and the scattering of surface waves by *single* isolated holes.

**KEYWORDS:** surface plasmon polariton · damping · lifetime · scattering · nanohole

*Address correspondence to hcong@phy.cuhk.edu.hk, s.maier@imperial.ac.uk.

Received for review September 28, 2009 and accepted December 10, 2009.

**Published online December 22, 2009.** 10.1021/nn901310k



Since the experimental observation of the phenomenon of extraordinary optical transmission[1] and the theoretical demonstration of the occurrence of superlensing in negative index materials,[2] many research efforts have been focused on exploring how surface plasmon polaritons (SPPs) allow the control of the flow of light at the nanoscale.[3] The emerging field of plasmonics[4] encompasses all of these studies devoted to analyze the interaction of light with metal nanostructures and aims to exploit the ability of SPPs to confine and transport electromagnetic (EM) energy in the subwavelength regime.[5−8]

In this context, the resonant scattering of SPP modes at subwavelength metallic defects has become an object of intense study.[9] During the past decade, plasmonic resonances have been thoroughly analyzed in a great variety of geometries such as nanospheres,[10] nanodisks,[11] nanorods,[12] or nanoshells.[13] Specifically, due to their simplicity and versatility, the potential use of nanohole arrays has been explored in a broad range of technological areas. Current nanofabrication techniques have enabled the geometrical tuning of such structures, allowing an accurate tailoring of their electromagnetic response. Thus, metallic nanoholes have been theoretically proposed and experimentally tested as optical functional elements with applications in fields such as nanolithography,[14,15] imaging,[16] microscopy,[17] optical nanoantennas,[18] lasing technology,[19] or biosensing.[20,21]

The scattering of SPP modes on two-dimensional (2D) metallic nanostructures was first studied within theoretical frameworks which model the polarizability of the scatterers by their dipolar quasi-static value.[22−24] Note that this is equivalent to the so-called Rayleigh approximation,[25] which is only valid for scatterers whose dimensions are much smaller than the incoming wavelength. Subsequently, novel approaches have been developed to overcome this limitation, which has allowed the treatment of more complex scattering geometries[26,27] and also shed light on the properties of single holes.[28]

From the experimental side, scanning near-field microscopy has allowed exploration of the temporal decay behavior of SPPs excited by ultrashort laser pulses,[29] and emissivity far-field measurements have led to a deeper understanding of the scattering properties of single defects and particle arrays.[30−32] However, very few works have analyzed the correlation between the damping suffered by SPPs when traveling along metallic nanostructured surfaces and the spectral features appearing in far-field emissivity spectra.

Kim *et al.* have recently shown that Rayleigh-like scattering lies at the origin of the damping experienced by SPPs in perforated hole arrays. They observed that the line width of the peaks in the transmission spectra associated with SPP modes in such systems scales as $\lambda^{-4}$ (where $\lambda$ denotes the

impinging wavelength).[33] Motivated by these experiments, Müller *et al.* performed fully three-dimensional (3D) simulations on ultrafast light propagation through periodic nanohole arrays. They found that, for a given excitation wavelength, lifetimes associated with radiative damping are inversely proportional to the fourth power of the hole diameter for apertures much smaller than λ.[34] Rayleigh scattering of SPPs has been also verified in thin films perforated with chains of nanoholes much smaller than the excitation wavelength.[35] The limitations of the Rayleigh description of the scattering of SPPs by nanoholes have also been tested experimentally. Li *et al.*[36] have reported that the SPP lifetimes in holes of dimensions comparable to the wavelength follow a $\lambda^n$ behavior, where $n$ is enlarged with increasing hole radius from the Rayleigh scattering regime. This observation clearly indicates that higher multipolar modes are contributing to the nanoholes' EM response.

In this work, we study the λ-dependent SPP lifetimes on gold surfaces structured with 2D periodic arrays of blind holes. These are determined from the line widths of the reflectivity drops observed in the far-field spectra for such structures. Both experiments and calculations demonstrate a strong dependence on the hole radius, $R$, and depth, $h$. We show that, for a given hole geometry, lifetimes exhibit a $\lambda^n$ dependence, where the exponent $n$ is close to 4 for wavelengths much larger than the hole dimensions but is much larger than 4 at shorter wavelengths. On the other hand, at a constant λ, lifetimes for shallow holes feature little dependence on the radius, recovering the Rayleigh's $R^{-4}$ dependence reported for deeper holes. By means of a simple model based on the Mie theory for spherical particles, we discuss the validity of the Rayleigh approximation for SPP scattering at holes. Finally, we show that the lifetime behavior in such structures can be understood in terms of the scattering of SPPs at a *single* hole. In this picture, the rest of the hole array simply acts as a coupler which converts efficiently the incoming radiation into surface waves. Therefore, we can conclude that the far-field experimental technique presented here gives us access to the near-field features of the scattering between SPPs and single nanometric holes.

## RESULTS AND DISCUSSION

Figure 1a shows top and lateral (see inset) scanning electron microscopy (SEM) images of the experimental 2D nanohole arrays under study. We consider holes of radii ranging from 38 to 177 nm and depths between 60 and 510 nm, keeping the array period, $P$, fixed to 762 nm. Figure 1c shows the measured reflectivity spectra at four different angles, θ, for a hole array with $R = 177$ nm and $h = 300$ nm. We restrict our analysis to the wavelength range in which only the lowest (−1,0) SPP mode supported by the structure can be excited. As expected, the spectra show reflection dips which are redshifted with increasing θ, a clear indication of the excitation of SPPs in the nanostructured gold surface through grating−coupling.[37]

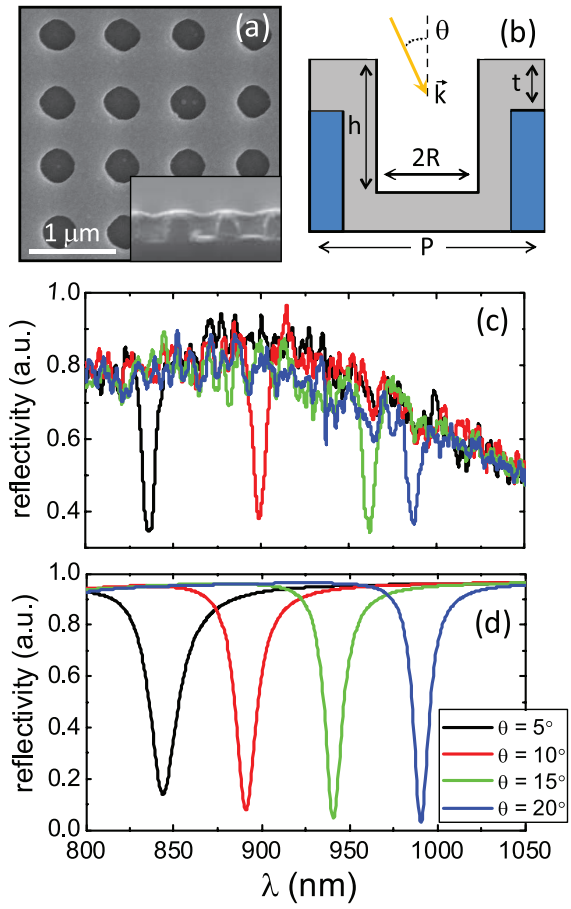


**Figure 1. (a) Top and lateral (inset) SEM images of the experimental sample with $R = 177$ nm and $h = 300$ nm. (b) Schematic view of the unit cell considered in the simulations and definition of the different geometric parameters of the structure. Gray (blue) regions correspond to the gold coating (photoresist layer). (c) Measured specular reflectivity spectra for $R = 177$ nm and $h = 300$ nm at four different incident angles. (d) Simulated reflection *versus* wavelength for the geometries considered in panel c.**

We have performed extensive FIT (finite integration technique) simulations on the experimental structures described above. The unit cell considered in the calculations is rendered in panel b of Figure 1. Specular reflectivity under TM polarization is calculated for the four incident angles considered in the experiments. Figure 1d plots the spectra obtained, which are in good agreement with the experimental data. Note that reflection drops in both panels become narrower for larger incident angles, which reveals the spectral sharpening of the SPP resonance with increasing wavelength.

To study the dependence of SPP resonances on λ, we have determined the full width at half-maximum (fwhm) of the reflection dips obtained from both experiments and simulations. This enables us to calculate the SPP lifetimes through the simple relation $\tau_{SP} = \hbar/\Gamma$ (where $\tau_{SP}$ is the SPP lifetime and Γ is the fwhm of the dip in energy units). We have fitted the spectra shown in Figure 1 to a Fano line shape function[38,39] of the form

$$y = y_0 + \frac{A\left(\frac{E - E_{res}}{\Gamma/2} + q\right)^2}{1 + \left(\frac{E - E_{res}}{\Gamma/2}\right)^2} \quad (1)$$

where $E$ and $E_{res}$ are the incoming and resonant energies, respectively, and $y_0$ is the offset function, which takes into account the reflection background. Coefficient $A$ describes the contribution of the zero-order continuum state coupled to the discrete resonant spectrum, and $q$ is the so-called Breit−Wigner−Fano coupling parameter.

Figure 2 plots the Fano-fitted lifetimes *versus* λ for two arrays of 300 nm deep holes with $R = 90$ nm (a) and $R = 177$ nm (b). As mentioned above, experiments and simulations show that, for a given geometry, SPP lifetimes increase with larger wavelength. Note that in both panels theory predicts larger lifetimes than those found in the experiments. This can be linked to the presence of defects and imperfections in the experimental samples, which scatter SPP waves out of the gold surface, reducing the measured $\tau_{SP}$. We analyze the dependence of SPP lifetimes on λ by fitting the two sets of experimental and theoretical results shown in Figure 2 to the expression

$$\tau_{SP} \propto \lambda^n \quad (2)$$

Fitted curves obtained for measured (simulated) data are plotted in black (red) in the figure. In panel a, $R = 90$ nm, the fitting parameter $n$ for both experiment and theory is around 4. This result agrees with previous studies and indicates that $\tau_{SP}$ is governed by Rayleigh-like scattering of SPPs at the holes.[33] However, for holes with $R = 177$ nm, $n$ increases to 7.4 in the wavelength range of experimental detection (see panel b). This implies that the SPP damping mechanism in this case is different and cannot be accurately described by the Rayleigh approximation. We have performed FIT simulations which confirm this behavior and predict the recovering of $n \simeq 4$ when extending the spectral range to larger wavelengths.

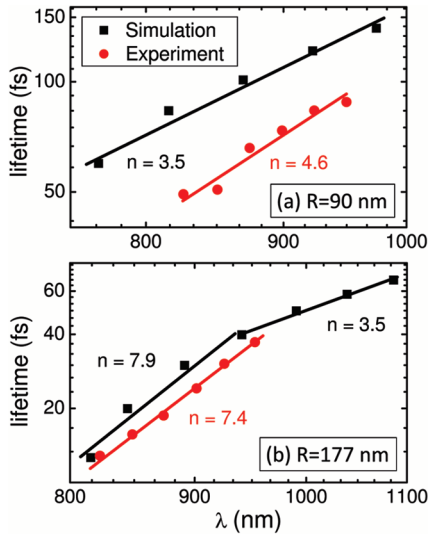


**Figure 2. Theoretical and experimental SPP lifetimes *versus* wavelength in log−log scale for hole arrays of depth $h$ = 300 nm and two different radii: 90 nm (a) and 177 nm (b). Solid lines plot fittings of the form $\tau_{SP} \propto \lambda^n$. Fitted values for the exponent $n$ are also shown.**

To gain physical insight into the complex behavior of $\tau_{SP}$ described above, we rely on a simple model which identifies two different contributions to the SPP damping in structured surfaces.[34] On the one hand, SPPs suffer losses due to intrinsic metal absorption. On the other hand, the scattering at the hole defects also leads to the decay of EM fields associated with SPPs. We can introduce characteristic lifetimes for these two damping effects: $\tau_{abs}$ (intrinsic absorption) and $\tau_{scat}$ (scattering losses). Thus, SPP lifetimes can be expressed in terms of these two contributions as

$$\frac{1}{\tau_{SP}} = \frac{1}{\tau_{abs}} + \frac{1}{\tau_{scat}} \quad (3)$$

We can estimate the dependence of $\tau_{abs}$ on the wavelength through the SPP decay length in flat metallic surfaces, $l_{abs} = \lambda \mathrm{Re}\{\varepsilon_M\}^2/(2\pi \mathrm{Im}\{\varepsilon_M\})$,[40] where $\varepsilon_M$ is the metal dielectric function. Taking the Drude-like permittivity presented in the Methods section, we have $\tau_{abs} \propto \lambda^2$ within the wavelength range considered in the experiments. Similarly, the behavior of $\tau_{scat}$ will be controlled by the scattering decay length $l_{scat}$. By imposing energy conservation at the scattering process between SPPs and a single hole (isolated from the rest of the array), we find the relation $\sigma_h/P + e^{-P/l_{scat}} = 1$ (where $\sigma_h$ is the hole cross section and $P$ the array period). Assuming that only a small part of the EM energy carried by the incoming SPPs is lost in each of these scattering events, we find that $l_{scat} \simeq P^2/\sigma_h$ and, hence, $\tau_{scat} \propto \sigma_h^{-1}$. We can anticipate that this term is going to govern $\tau_{SP}$ in eq 3, as SPPs interact with many holes before being absorbed and, therefore, $\tau_{scat} \ll \tau_{abs}$ in our experimental samples.

We model the cross section of the perforated holes by borrowing the Mie scattering theory for freestanding spherical particles.[41] It allows us to write the scattering cross section as $\sigma_h = (8\pi^3/3\lambda^4)|\alpha|^2$, where α denotes the particle polarizability.[42] By including only quadrupolar corrections to the Rayleigh quasi-static value, $\alpha_{Ray} = 4\pi a^3[(\varepsilon_M - 1)/(\varepsilon_M + 2)]$ (where $a$ is the particle radius), we can write $\alpha = \alpha_{Ray}[1 - 0.6((\varepsilon_M - 2)/(\varepsilon_M + 2))(2\pi a/\lambda)^2]$.[10] Note that, in the frequency range of interest, $|\varepsilon_M| \gg 2$, and therefore, the dependence of the scatterer polarizability on λ is explicitly shown by the expressions above. We transfer this theoretical framework to blind holes by introducing the phenomenological parameter $a_c = ((3/4)R^2h)^{1/3}$, which corresponds to the radius of spherical particles of the same volume as cylindrical holes of radius $R$ and depth $h$.

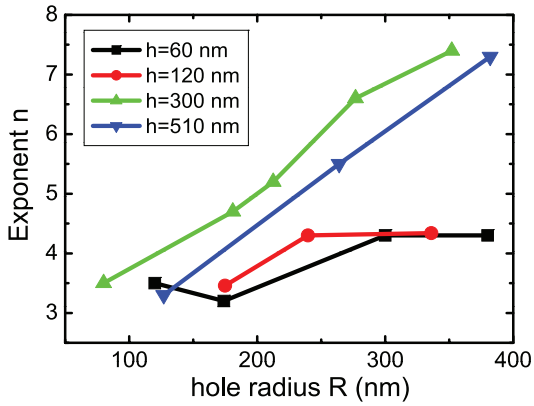


**Figure 3. Exponent *n* as a function of *R* obtained by fitting experimental SPP lifetimes at wavelengths between 800 and 1100 nm. Structures with four different hole depths are shown.**

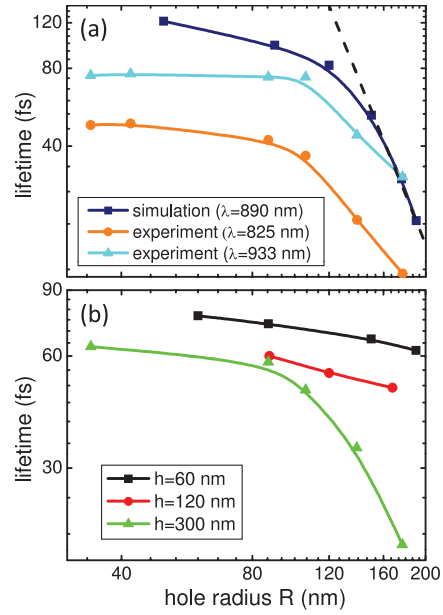


**Figure 4. (a) Experimental and simulated SPP lifetimes as a function of the hole radius at three different wavelengths and for $h = 300$ nm. Black dotted line plots the $R^{-4}$ dependence predicted by Rayleigh approximation. (b) Experimental SPP lifetimes at $\lambda = 875$ nm *versus* *R* for three different hole depths.**

The simple approach described above reproduces the behavior of SPP lifetimes shown in Figure 2. For $R = 90$ nm, $2\pi a_c = 770$ nm is much smaller than the wavelength range spanned in panel a. Thus, the Rayleigh approximation, which yields $\tau_{SP} \simeq \tau_{scat} \propto \lambda^4$, describes accurately the tendency extracted from the experimental and simulated data ($n \simeq 4$). However, for $R = 177$ nm, $2\pi a_c = 1200$ nm, which means that higher order corrections to $\sigma_h$ play a relevant role. In this case, our model predicts the appearance of a $\lambda^8$ contribution in $\tau_{SP}$, which is enlarged with decreasing $\lambda$. This result agrees with the fitted values obtained for Figure 2b, which gives $n \simeq 4$ ($n \simeq 8$) at large (small) wavelengths.

In order to further explore how the hole geometry affects SPP lifetimes, we have studied experimentally the variation of the fitting exponent *n* in eq 2 with the hole radius and depth. Figure 3 plots *n* *versus* *R* for four different hole depths. Notice that the fitting procedure leading to the results shown in the figure has been carried out for the spectral range between 800 and 1100 nm. We can see that in the case of shallow holes ($h =$ 60, 120 nm) *n* is around 4 for all of the radii analyzed. This evidence that Rayleigh-like scattering governs SPP lifetimes is consistent with the fact that $2\pi a_c < \lambda$ for these two sets of geometric parameters. However, when deeper holes are considered ($h = 300$, 510 nm), *n* deviates from 4 as *R* increases. Again, this effect can be linked to the presence of higher multipolar contributions to the holes' cross section. Note that the highest value for *n* found in the experiments is close to 8, which agrees with the $\lambda^8$ dependence that our model yields for quadrupolar corrections to $\tau_{scat}$.

Up to here, we have focused on describing the dependence of eq 2 on the radius and depth of the perforated holes. However, we have not yet examined how SPP lifetimes are modified at a constant wavelength by the hole geometry. Recent experimental[33] and theoretical[34] studies have reported an $R^{-4}$ dependence of $\tau_{SP}$ in subwavelength hole arrays. In all of these works, SPP lifetimes were investigated through the transmission properties of perforated metallic films. Our theoretical model gives $\sigma_h \propto R^4h^2$ within the Rayleigh approximation, which agrees with these previous observations. However, it is worthy to analyze if the same dependence holds in our reflection configuration.

Figure 4a renders experimental and simulated SPP lifetimes as a function of the hole radius ($h = 300$ nm) at three different wavelengths. The black dotted line plots the $R^{-4}$ behavior predicted by Rayleigh scattering. We can see that this theoretical result is only valid for $R > 150$ nm within the radius range considered in the figure. Note that the little deviation from this prediction displayed by measured SPP lifetimes at $R > 150$ nm can be linked to irregularities in the experimental hole radii. The apparent failure of the Rayleigh approximation observed in Figure 4a at smaller *R*, where it should be very accurate, indicates that the main contribution to SPP lifetimes in eq 3 is not given by $\tau_{scat}$ but by $\tau_{abs}$. This can be understood as a result of the small interaction of SPPs traveling on the metal surface with deeply subwavelength holes. This increases the characteristic scattering lifetime which becomes comparable to that associated with absorption losses at the flat regions of the structure. Importantly, $\tau_{abs}$ in our model is independent of the hole geometry. Thus, from Figure 4a, we can infer that, for $R < 80$ nm, absorption losses control SPP lifetimes, which translates into the fact that they become independent of the size of the holes perforated on the metal surface.

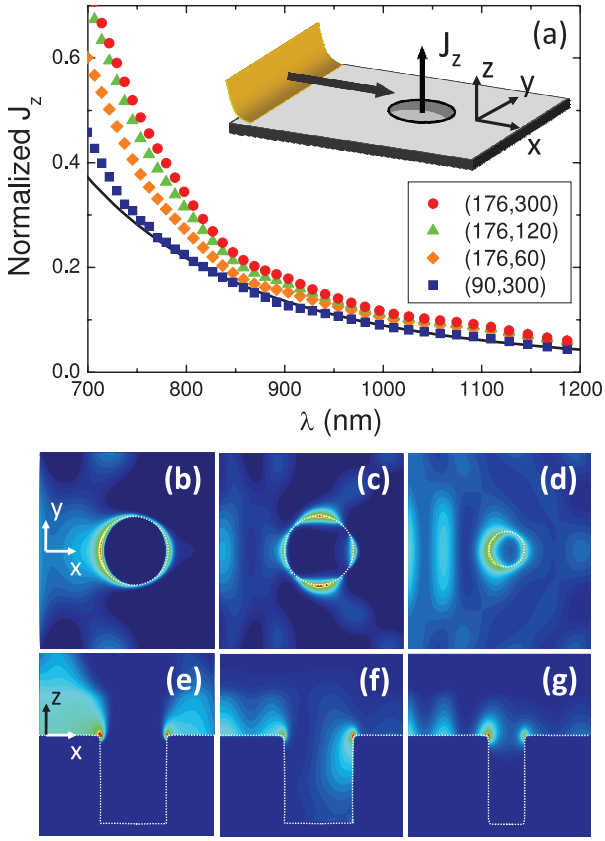


**Figure 5. (a) Wavelength dependence of the normalized out-of-plane emissivity, $J_z$ for four different hole geometries labeled by ($R$, $h$), the hole radius and depth in nanometers. Black solid line plots the Rayleigh's $\lambda^{-4}$ behavior. Bottom panels render the electric field amplitude $|E|$ at different planes for $h = 300$ nm. (b,e) $|E|$ for holes with $R = 177$ nm at $\lambda = 1150$ nm. (c,f) Correspond to the same structure at $\lambda = 700$ nm. (d,g) Evaluated at $\lambda = 700$ nm for holes with $R = 90$ nm.**

We test our conclusion about absorption effects in SPP lifetimes for deep subwavelength holes by studying their behavior for different hole depths. In Figure 4b, we have plotted $\tau_{SP}$ *versus* $R$ at $\lambda = 875$ nm for three different hole depths. As expected, for shallow holes ($h = 60$, 120 nm), SPP lifetimes are almost independent of the hole radius. However, when the hole depth increases, $\tau_{scat}$ is reduced and acquires the main role in eq 3. This makes SPP lifetimes recover their dependence on the hole radius, as clearly shown by the experimental data for $h = 300$ nm.

We check the validity of our simple model (based on the Mie theory for spherical particles) for describing the scattering properties of nanoholes within the range of geometries and wavelengths considered in our experiments. For this purpose, we have performed FDTD simulations on the scattering of SPPs at a single cylindrical hole on a gold surface (see inset of Figure 5a). We introduce here the emissivity $J_z$, which corresponds to the out-of-plane EM power flowing through the hole area normalized to the EM energy impinging on it. Figure 5a shows $J_z$ *versus* wavelength for four different hole geometries. The hole dimensions are labeled as ($R$, $h$), where $R$ and $h$ are the hole radius and depth, respectively, in nanometers. For comparison, we have also plotted as a black solid line the $\lambda^{-4}$ dependence yielded by the Rayleigh approximation for spherical particles. For all of the structures, $J_z$, which governs the scattering cross section of the holes, is proportional to $\lambda^{-4}$ only at long wavelengths. For decreasing $\lambda$, $J_z$ grows faster than Rayleigh's prediction, and the spectral position at which this deviation occurs is shifted to shorter $\lambda$ for smaller holes. This behavior is consistent with our model, in which multipolar contributions in $\sigma_h$ become more important as the effective radius $a_c$ increases. Note that at a constant wavelength a reduction on $h$ or $R$ translates into $J_z$ approaching the $\lambda^{-4}$ dependence.

In order to verify that the failure of the Rayleigh approximation for single holes is due to the excitation of higher multipolar modes in the scattering process, we render in the lower panels of Figure 5 the electric field amplitude, $|E|$, at different planes of the structure with $h = 300$ nm. Panels b and e are evaluated at $\lambda = 1150$ nm for a hole radius of 177 nm. As expected, for this set of parameters, the field pattern has a strong dipolar character. However, $|E|$ in panels c and f, which corresponds to the same geometry but at $\lambda = 700$ nm, demonstrates the appearance of a quadrupolar mode at the hole opening, which explains why Rayleigh theory is not valid in this case. Note that fields in panel f penetrate into the hole, which indicates that it supports propagating modes at this wavelength. In order to check this point, we have calculated the cutoff wavelength for the lowest ($TE_{11}$) mode supported by the holes, finding that, for the $\varepsilon_M$ described in the Methods section, it is equal to 733 nm. Finally, panels d and g render the electric field amplitude for $\lambda = 700$ nm and $R = 90$ nm. These demonstrate that the recovery of Rayleigh scattering in the system is linked to the presence of a strongly dipolar field distribution at the hole. Note that in this case fields do not explore the depth of the hole, as the theoretical cutoff wavelength for this radius (490 nm) is much smaller than $\lambda$.

## CONCLUSION

In conclusion, we have studied through both experiments and simulations surface plasmon polariton lifetimes on periodic arrays of blind holes on a gold surface. We have analyzed their dependence on the wavelength and the hole geometry through reflectivity measurements. We have developed a simple model based on the Mie scattering for freestanding particles which reproduces all of the phenomenology extracted from our observations. Finally, we have checked that the conclusions that we raise from our model with regard to the validity of the Rayleigh approximation are consistent with exact calculations on the scattering of SPPs with single holes.

## METHODS

**Experiments.** The fabrication techniques and measurement method considered are explained elsewhere.[36,43] Briefly, the experimental 2D nanohole arrays were fabricated by interference lithography on SU-8 negative photoresist layers in which two parameters were used to control the holes' geometry: the layer thickness and the exposure time. Once the hole layer structures were built, a $t = 100$ nm thick Au film was deposited at room temperature on the photoresist by sputtering. We fixed the array period to 762 nm while varying the hole radius from 38 to 177 nm. Nanoholes with depths ranging from 60 to 510 nm were built. Angle-dependent reflectivity measurements were performed by using a homemade automated goniometer. Samples were illuminated by a collimated and linearly polarized white light, and the specular reflection was captured by charge-coupled device-based detection.

**Theory.** Specular reflection spectra for 2D nanohole arrays with the same dimensions as the experimental samples were obtained using the CST MICROWAVE STUDIO software implementing the finite integration technique (FIT). The scattering of SPPs at single blind holes on a flat gold surface were calculated through LUMERICAL, a commercial finite-difference time domain (FDTD) code. In our simulations, we have modeled the EM response of gold through a Drude-like dielectric function of the form

$$\varepsilon_M(\omega) = \varepsilon_\infty - \frac{\omega_p^2}{\omega(\omega + i\gamma)} \quad (4)$$

where $\varepsilon_\infty = 10.7026$ is the high-frequency limit dielectric constant, and $\omega_p = 1.3748 \times 10^{16}$ rad/s and $\gamma = 1.1738 \times 10^{14}$ rad/s, the plasma and damping frequencies, respectively. These Drude parameters were obtained by fitting experimental values[44] at the wavelength range of interest. We have characterized the photoresist layer with $\varepsilon = 2.43$.

*Acknowledgment.* D.Y.L., A.I.F.-D., and S.A.M. acknowledge support from UK Engineering and Physical Sciences Research Council (EPSRC). J.L. and H.C.O. acknowledge support from the Chinese University of Hong Kong through the RGC Competitive Earmarked Research Grants (402807 and 402908) and the Shun Hing Institute of Advanced Engineering (BME-p2-08).

## REFERENCES AND NOTES

1. Ebbesen, T. W.; Lezec, H. J.; Ghaemi, H. F.; Thio, T.; Wolff, P. A. Extraordinary Optical Transmission through Subwavelength Hole Arrays. *Nature* **1998**, *391*, 667.
2. Pendry, J. B. Negative Refraction Makes a Perfect Lens. *Phys. Rev. Lett.* **2000**, *85*, 3966.
3. Barnes, W. L.; Dereux, A.; Ebbesen, T. M. Surface Plasmon Subwavelength Optics. *Nature* **2003**, *424*, 824.
4. Maier, S. A. *Plasmonics: Fundamentals and Applications*; Springer: New York, 2007.
5. Ebbesen, T. M.; Genet, C.; Bozhevolnyi, S. I. Surface-Plasmon Circuitry. *Phys. Today* **2008**, *61*, 44.
6. Atwater, H. A. The Promise of Plasmonics. *Sci. Am.* **2007**, *296*, 56.
7. Lal, S.; Link, S.; Halas, N. J. Nano-Optics from Sensing to Waveguiding. *Nat. Photonics* **2007**, *1*, 461.
8. Maier, S. A. Plasmonics: Metal Nanostructures for Subwavelength Photonic Devices. *IEEE J. Sel. Top. Quantum Electron.* **2006**, *12*, 1214.
9. Zayats, A. V.; Smolyaninov, I. I.; Maradudin, A. A. Nano-Optics of Surface Plasmon Polaritons. *Phys. Rep.* **2005**, *408*, 131.
10. Myroshnychenko, V.; Rodríguez-Fernández, J.; Pastoriza-Santos, I.; Funston, A. M.; Novo, C.; Mulvaney, P.; Liz-Marzán, L. M.; de Abajo, F. J. G. Modelling the Optical Response of Gold Nanoparticles. *Chem. Soc. Rev.* **2008**, *37*, 1793.
11. Kravets, V. G.; Schedin, F.; Grigorenko, A. N. Extremely Narrow Plasmon Resonances Based on Diffraction Coupling of Localized Plasmons in Arrays of Metallic Nanoparticles. *Phys. Rev. Lett.* **2008**, *101*, 087403.
12. Auguié, B.; Barnes, W. L. Collective Resonances in Gold Nanoparticle Arrays. *Phys. Rev. Lett.* **2008**, *101*, 143902.
13. Oldenburg, S. J.; Averitt, R. D.; Westcott, S. L.; Halas, N. J. Nanoengineering of Optical Resonances. *Chem. Phys. Lett.* **1998**, *288*, 243.
14. Luo, X.; Ishihara, T. Surface Plasmon Resonant Interference Nanolithography Technique. *Appl. Phys. Lett.* **2004**, *84*, 4780.
15. Srituravanich, W.; Pan, L.; Wnag, Y.; Sun, C.; Bogy, D. B.; Zhang, X. Flying Plasmonic Lens in the Near Field for High-Speed Nanolithography. *Nat. Nanotechnol.* **2008**, *3*, 733.
16. Laux, E.; Genet, C.; Skauli, T.; Ebbesen, T. W. Plasmonic Photon Sorters for Spectral and Polarimetric Imaging. *Nat. Photonics* **2008**, *2*, 161.
17. Brun, M.; Drezet, A.; Mariette, H.; Chevalier, N.; Woehl, J. C.; Huant, S. Remote Optical Addressing of Single Nano-Objects. *Europhys. Lett.* **2003**, *64*, 634.
18. Alaverdyan, Y.; Sepúlveda, B.; Eurenius, L.; Olsson, E.; Käll, M. Optical Antennas Based on Coupled Nanoholes in Thin Metal Films. *Nat. Phys.* **2007**, *3*, 884.
19. Yu, N.; Fan, J.; Wang, Q. J.; Pflügl, C.; Diehl, L.; Edamura, T.; Yamanishi, M.; Kan, H.; Capasso, F. Small-Divergence Semiconductor Lasers by Plasmonic Collimation. *Nat. Photonics* **2008**, *2*, 564.
20. Stewart, M. E.; Anderton, C. R.; Thompson, L. B.; Maria, J.; Gray, S. K.; Rogers, J. A.; Nuzzo, R. G. Nanostructured Plasmonic Sensors. *Chem. Rev.* **2008**, *108*, 494.
21. Anker, J. N.; Hall, W. P.; Lyandres, O.; Shah, N. C.; Zhao, J.; Duyne, R. P. V. Biosensing with Plasmonic Nanosensors. *Nat. Mater.* **2008**, *7*, 442.
22. Shchegrov, A. V.; Novikov, I. V.; Maradudin, A. A. Scattering of Surface Plasmon Polaritons by a Circularly Symmetric Surface Defect. *Phys. Rev. Lett.* **1997**, *78*, 4269.
23. Xiao, M.; Zayats, A.; Siqueiros, J. Scattering of Surface-Plasmon Polaritons by Dipoles Near a Surface: Optical Near-Field Localization. *Phys. Rev. B* **1997**, *55*, 1824.
24. Evlyukhin, A. B.; Bozhevolnyi, S. I. Surface Plasmon Polariton Scattering by Small Ellipsoid Particles. *Surf. Sci.* **2005**, *590*, 173.
25. Jackson, J. D. *Classical Electrodynamics*, 3rd ed.; John Wiley & Sons: New York, 1999.
26. Evlyukhin, A. B.; Brucoli, G.; Martin-Moreno, L.; Bozhevolnyi, S. I.; Garcia-Vidal, F. J. Surface Plasmon Polariton Scattering by Finite-Size Nanoparticles. *Phys. Rev. B* **2007**, *76*, 075426.
27. de Leon-Perez, F.; Brucoli, G.; Garcia-Vidal, F. J.; Martin-Moreno, L. Theory on the Scattering of Light and Surface Plasmon Polaritons by Arrays of Holes and Dimples in a Metal Film. *New J. Phys.* **2008**, *10*, 105017.
28. Park, T. H.; Mirin, N.; Lassiter, J. B.; Nehl, C. L.; Halas, N. J.; Nordlander, P. Optical Properties of a Nanosized Hole in a Thin Metallic Film. *ACS Nano* **2008**, *2*, 25.
29. Ropers, C.; Park, D. J.; Stibenz, G.; Steinmeyer, G.; Kim, J.; Kim, D. S.; Lienau, C. Femtosecond Light Transmission and Subradiant Damping in Plasmonic Crystals. *Phys. Rev. Lett.* **2005**, *94*, 113901.
30. Hecht, B.; Bielefeldt, H.; Novotny, L.; Inouye, Y.; Pohl, D. W. Local Excitation, Scattering and Interference of Surface Plasmons. *Phys. Rev. Lett.* **1996**, *77*, 1889.
31. Sönnichsen, C.; Duch, A. C.; Steininger, G.; Koch, M.; von Piessen, G.; Feldmann, J. Launching Surface Plasmons into Nanoholes in Metal Films. *Appl. Phys. Lett.* **2000**, *76*, 140.
32. García de Abajo, F. J. Colloquium: Light Scattering by Particle and Hole Arrays. *Rev. Mod. Phys.* **2007**, *79*, 1267.
33. Kim, D. S.; Hohng, S. C.; Malyarchuk, V.; Yoon, Y. C.; Ahn, Y. H.; Yee, K. J.; Park, J. W.; Kim, J.; Park, Q. H.; Lienau, C. Microscopic Origin of Surface-Plasmon Radiation in Plasmonic Band-Gap Nanostructures. *Phys. Rev. Lett.* **2003**, *91*, 143901.
34. Müller, R.; Malyarchuk, V.; Lienau, C. Three-Dimensional Theory on Light-Induced Near-Field Dynamics in a Metal Film with a Periodic Array of Nanoholes. *Phys. Rev. B* **2003**, *68*, 205415.

35. Alaverdyan, Y.; Hempe, E.-M.; Vamivakas, A. N.; Haibo, E.; Maier, S. A.; Atatüre, M. Spectral and Angular Distribution of Rayleigh Scattering from Plasmon-Coupled Nanohole Chains. *Appl. Phys. Lett.* **2009**, *94*, 021112.
36. Li, J.; Iu, H.; Lei, D. Y.; Wan, J. T. K.; Xu, J. B.; Ho, H. P.; Waye, M. Y.; Ong, H. C. Dependence of Surface Plasmon Lifetimes on the Hole Size in Two-Dimensional Metallic Arrays. *Appl. Phys. Lett.* **2009**, *94*, 183112.
37. Raether, H. *Surface Plasmons*; Springer: Berlin, 1988.
38. Genet, C.; van Exter, M. P.; Woerdman, J. P. Fano-Type Interpretation of Red Shifts and Red Tails in Hole Array Transmission Spectra. *Opt. Commun.* **2003**, *225*, 331.
39. Li, J.; Xu, J. B.; Ong, H. C. Hole Size Dependence of Forward Emission from Organic Dyes Coated with Two-Dimensional Metallic Arrays. *Appl. Phys. Lett.* **2009**, *94*, 241114.
40. Barnes, W. L. Surface Plasmon-Polariton Length Scales: A Route to Subwavelength Optics. *J. Opt. A: Pure Appl. Opt.* **2006**, *8*, S87.
41. Mie, G. Beiträge zur Optik trüber Medien, Speziell Kolloidaler Metallösungen. *Ann. Phys. (Leipzig)* **1908**, *25*, 377.
42. Novotny, L.; Hecht, B. *Principles of Nano-Optics*; Cambridge University Press: New York, 2006.
43. Li, J.; Iu, H.; Luk, W. C.; Wan, J. T. K.; Ong, H. C. Studies of the Plasmonic Properties of Two-Dimensional Metallic Nanobottle Arrays. *Appl. Phys. Lett.* **2008**, *92*, 213106.
44. Johnson, P. B.; Christy, R. W. Optical Constants of the Noble Metals. *Phys. Rev. B* **1972**, *6*, 4370.